An efficient method for removal of pentachlorophenol using adsorption and microwave regeneration with different magnetic carbon nanotubes

Xue Zhang, Chunyue Cui, Ying Wang, Jing Chang, Dong Ma and Jing Wang

ABSTRACT

Various magnetic carbon nanotubes (CNTs) $Co_{0.5}M_{0.5}Fe_2O_4$-CNTs (M = Cu, Mn, Ni, Zn) were successfully prepared and applied for treatment of pentachlorophenol (PCP) with adsorption and microwave irradiation process. The $Co_{0.5}M_{0.5}Fe_2O_4$-CNTs were characterized by transmission electron microscopy, X-ray diffraction, vibrating sample magnetometry, and microwave absorption spectroscopy. The adsorption experiment results showed the adsorption capacity for PCP was in the following order: $Co_{0.5}Cu_{0.5}Fe_2O_4$-CNTs > $Co_{0.5}Mn_{0.5}Fe_2O_4$-CNTs > $Co_{0.5}Ni_{0.5}Fe_2O_4$-CNTs > $Co_{0.5}Zn_{0.5}Fe_2O_4$-CNTs. After adsorption, the $Co_{0.5}M_{0.5}Fe_2O_4$-CNTs was separated by magnetic field and regenerated by microwave irradiation at 850 W for 180 s. It was confirmed that after six adsorption and microwave regeneration cycles, the regeneration efficiency maintained over 90%. In particular, $Co_{0.5}Cu_{0.5}Fe_2O_4$-CNTs exhibited excellent adsorption capacity and reusability. These results can open a new avenue for treatment of chlorinated organic compounds with efficiently and non-secondary pollution.

Key words | adsorption, magnetic carbon nanotubes, microwave regeneration, pentachlorophenol

Xue Zhang
Chunyue Cui (corresponding author)
Ying Wang
Jing Chang
Dong Ma
Jing Wang
School of Resource and Environment,
Qingdao Agricultural University,
Qingdao 266109,
China
E-mail: *cuichunyue1977@163.com*

INTRODUCTION

Polychlorinated organic compounds constitute a major group of environmental pollutants, with widespread application in the chemical, pharmaceutical, agricultural, and leather industries (Weavers *et al.* 2000). Polychlorinated organic compounds are highly toxic and persistent in the environment and highly resistant to environmental degradation. Therefore, it is highly desirable to develop an efficient treatment of polychlorinated organic compounds that involves no secondary pollution.

Some technologies, such as biodegradation processes (Zhu *et al.* 2012), chemical oxidation (Ye *et al.* 2010), adsorption (Peng *et al.* 2016), and electrochemical methods (Alfaya *et al.* 2015) have been proposed to treat polychlorinated organic compounds; however, each method has its own limitations and disadvantages. The coupling of technologies for treatment can overcome the weaknesses of one technology by acquiring the strong points of another technology to achieve the purpose of efficient treatment.

Adsorption is one of the most powerful techniques for the removal of organic compounds from wastewater because of its simple and easy operation and high efficiency (Mohammadi & Veisi 2018). However, adsorption is unable to degrade pollutants and so is only able to transfer the pollution. For treatment of pollutants without secondary contamination, adsorption therefore needs to be combined with another technology.

Microwave irradiation has been applied in the treatment of contaminated soil or wastewater in a process that is fast with no secondary pollution (Kahar *et al.* 2017; Qi *et al.* 2017). However, water can absorb microwaves and so most of the energy is absorbed by water, which means a lot of energy is wasted. It is therefore more energy efficient if the pollutant can be adsorbed onto microwave absorption materials for treatment.

In this study, a combination of adsorption and microwave technology is designed for the rapid treatment of chlorinated organic compounds. For this coupling of technologies, the key is the development of materials with high adsorption capacity, fast separation, and absorption of microwaves.

Carbon nanotubes (CNTs) are suitable as potential materials for the coupled technology treatment. Many studies have shown that CNTs have an excellent effect on the removal of organic pollutants from wastewater (Shao *et al.* 2010; Xiao *et al.* 2014; Bhanjana *et al.* 2017). To solve the problem of

doi: 10.2166/wst.2020.146

separating CNTs, there have been reports that the magnetic materials can load on the surface of CNTs, which facilitates efficient separation under the action of external magnetic fields (Peng *et al.* 2005; Gao *et al.* 2013; Wang *et al.* 2014).

The magnetic material ferrite is an excellent electromagnetic wave absorbing material (Kaiser 2012). The composite of ferrite magnetic materials and CNTs can therefore effectively improve the absorption microwave capabilities (Zhan *et al.* 2011; Wen *et al.* 2013). Among the various magnetic materials $CoFe_2O_4$ has good microwave absorption abilities (Li *et al.* 2015; Yan *et al.* 2015). If $CoFe_2O_4$ can be composited with other metals and loaded onto, CNT can increase its magnetism and microwave absorption abilities, which are more suitable for the adsorption–microwave combined treatment of organic matter in water. However, there has been little research in this area.

Based on the above research, in this study, Co_xM_y (M = Cu, Mn, Ni, Zn) Fe_2O_4 ferrite was selected and loaded onto the surface of CNTs for use in the adsorption–microwave irradiation coupled treatment for chlorinated organic compounds in water. The influencing factors and intrinsic relationship of the structure and composition of the adsorbed materials on the adsorption–microwave irradiation treatment are discussed.

METHODS

Preparation and modification of CNTs

The CNTs were synthesized by catalytic pyrolysis according to our previous report (Cui *et al.* 2008). They were grown at 900 °C for 2 h with a ferrocene–xylene mixture (Fe/C = 0.4%) as a catalyst and carbon source. The mixture gas was Ar and H_2 (9:1), which was flowed at a rate of 1,000 mL min^{-1}). The obtained CNTs were modified with a 4.0 M H_2SO_4–HNO_3 (1:1) mixture at 120 °C for 8 h under reflux. The modified CNTs were washed with deionized water and dried at 100 °C under vacuum and stored in a desiccator for use.

Preparation of magnetic CNTs (MCNTs)

First, 0.5 g of CNTs were fully dispersed in solutions of $Fe(NO_3)_3{\cdot}9H_2O$, $Co(NO_3)_2{\cdot}6H_2O$, $Ni(NO_3)_2{\cdot}6H_2O$ $CuSO_4{\cdot}5H_2O$, $MnSO_4{\cdot}H_2O$, $ZnSO_4{\cdot}7H_2O$. The molar ratio of Co:M (M = Ni, Cu, Mn. Zn): Fe was 1:1:5 and the magnetic material load was 20%. Second, an ethylene glycol and polyethylene glycol (the volume ratio was 1:50) mixture as a sediment agent was added. The mixture was ultrasonicated and placed in an autoclave and heated for 12 h at 180 °C. After cooling to room temperature, the precipitate was isolated using a permanent magnet and was washed with absolute ethanol, filtered, dried in a drying oven at 45 °C for 24 h, and bottled for use.

Adsorption experiment

To evaluate the adsorbability of the different MCNTs for pentachlorophenol (PCP) from the aqueous solutions, the adsorption experiment was carried out using the batch technique. The $Co_{0.5}M_{0.5}Fe_2O_4$-CNTs (M = Cu, Mn, Ni, Zn) were added to a flask that contained 50 mL of PCP solution and this was placed in a thermostatic shaker (200 rpm, 25 °C) for adsorption. The concentration of PCP was measured by high performance liquid chromatography (HPLC) and the amount of adsorption was calculated according to:

$$G = \frac{(C_0 - C_t)\,V}{m} \tag{1}$$

where G (mg g^{-1}) is adsorption capacity, C_0 (mg mL^{-1}) is the initial concentration, C_t (mg mL^{-1}) is the remaining concentration of PCP at any given time, V (mL) is the volume of solution, and m (g) is the mass of sorbents.

Microwave treatment

The MCNTs (1 g) were added to a flask that contained 100 mL of PCP solution (250 mg L^{-1}) and this was shaken in a thermostatic shaker (25 °C, 180 rpm) for 2 h to achieve adsorption equilibrium. The saturated MCNTs were treated with microwave set to 850 W with a frequency of 2,450 MHz. A schematic diagram of the microwave experimental apparatus is shown in our previous work (Cui *et al.* 2015).

The regeneration efficiency is an important index to determine the adsorption capacity of the magnetic CNTs. The formula is as follows:

$$\eta = \frac{G_W}{G_0} \times 100\% \tag{2}$$

where η is the regeneration efficiency, G_0 (mg g^{-1}) is the saturation adsorption capacity of newly prepared MCNTs and G_W (mg g^{-1}) is the saturation adsorption capacity after microwave irradiation treatment.

Analysis

The morphology of MCNTs was characterized by transmission electron microscopy (TEM, HT7700, Japan) and X-ray diffractometry (XRD, LabxXRD-6000, Shimadzu, Japan). Sample magnetic properties were determined using a vibrating sample magnetometer (Riken Denshi, BHV-525). The Brunauer–Emmett–Teller (BET) specific surface area was determined through nitrogen adsorption–desorption measurements (Autosorb-iQ-MP-VP, USA). The microwave absorption performance was analyzed using a microwave network analyzer (VNA, N5244A PNA-X, Agilent, USA). The composition of the magnetic materials was determined using inductively coupled plasma atomic emission spectroscopy (Advantage, IRIS, USA).

The concentration of PCP was analyzed using HPLC (Agilent, 1200 USA) equipped with a C_{18} reversed phase column (250 mm × 4.6 mm, 5 μm) and an ultraviolet detector (UV-1575). The degree of mineralization of PCP was determined using a total organic carbon (Liqui TOC trace, Elementar, Germany) analyzer.

RESULTS AND DISCUSSION

Morphology and microstructure of MCNTs

The morphological structures and composition of the different MCNTs were detected by TEM and energy-dispersive X-ray spectroscopy (EDX) (Figure 1). As shown in Figure 1(a), the CNTs diameter was 60–100 nm with a smooth surface, and the $Co_{0.5}Cu_{0.5}Fe_2O_4$ nanoparticles were spherical in shape with a diameter of 30–50 nm and were distributed uniformly on the CNTs. The EDX spectrum exhibited peaks

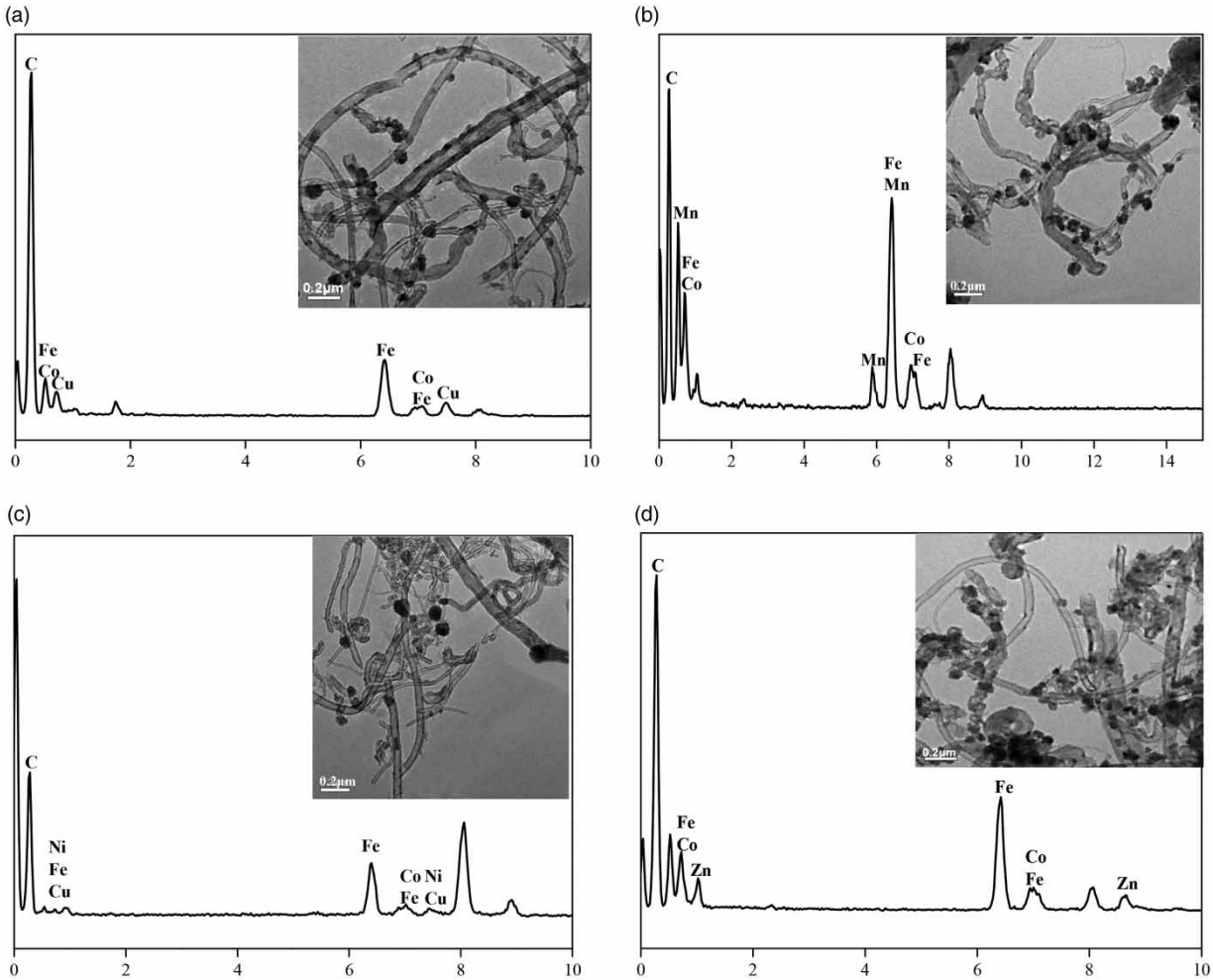

Figure 1 | TEM images of the different MCNTs: (a) $Co_{0.5}Cu_{0.5}Fe_2O_4$-CNTs; (b) $Co_{0.5}Mn_{0.5}Fe_2O_4$-CNTs; (c) $Co_{0.5}Ni_{0.5}Fe_2O_4$-CNTs; and (d) $Co_{0.5}Zn_{0.5}Fe_2O_4$-CNTs.

attributed to Co, Cu, Fe, and C. Figure 1(b) shows the TEM morphology and distribution of $Co_{0.5}Mn_{0.5}Fe_2O_4$ nanoparticles on the CNTs. The $Co_{0.5}Mn_{0.5}Fe_2O_4$ nanoparticles were dispersed uniformly on the CNTs with a diameter of 50–70 nm. The compositions of the $Co_{0.5}Mn_{0.5}Fe_2O_4$-CNT_S were determined from the EDX spectrum showing Co, Mn, Fe, and C. As shown in Figure 1(c), the $Co_{0.5}Ni_{0.5}Fe_2O_4$ nanoparticles were spherical in shape with an average diameter of 70 nm. The compositions of the $Co_{0.5}Ni_{0.5}Fe_2O_4$-CNT_S were determined by EDX experiments and Co, Ni, Fe, and C elements were mainly observed. The morphologies of the $Co_{0.5}Zn_{0.5}Fe_2O_4$-CNTs are shown in Figure 1(d). $Co_{0.5}Zn_{0.5}Fe_2O_4$ nanoparticles were dispersed uniformly on the CNTs with a diameter of 40–70 nm. Co, Zn, Fe, and C elements were mainly observed.

The XRD spectra of the CNTs $Co_{0.5}Cu_{0.5}Fe_2O_4$-CNTs, $Co_{0.5}Mn_{0.5}Fe_2O_4$-CNTs, $Co_{0.5}Ni_{0.5}Fe_2O_4$-CNTs, and $Co_{0.5}Zn_{0.5}Fe_2O_4$-CNTs are shown in Figure 2. A peak was observed at 26.03° from the XRD patterns in Figure 3(a), which corresponded to the (002) crystal of the CNTs. Compared with the CNTs, no new diffraction peaks were observed after loading with the magnetic material. As shown in the figure, the pure magnetic nanomaterials were amorphous. This proved that the magnetic material on CNT was amorphous.

Figure 3 shows the magnetic response characterization of the different MCNTs. The MCNTs, as adsorbents, were well dispersed in water and maintained a stable state (Figure 3(a)). When an external magnetic field was applied, the different MCNTs were attracted toward the magnet in a very short time (Figure 3(b)), which demonstrated a high magnetic sensitivity. Figure 3(c) shows the hysteresis loops of four magnetic CNTs at room temperature. As revealed in the figure, the magnetization increased with an increasing magnetic field for the different MCNTs at 298 K. The saturation magnetization of $Co_{0.5}Cu_{0.5}Fe_2O_4$-CNTs, $Co_{0.5}Mn_{0.5}Fe_2O_4$-CNTs, $Co_{0.5}Ni_{0.5}Fe_2O_4$-CNTs, and $Co_{0.5}Zn_{0.5}Fe_2O_4$-CNTs were 0.42, 0.61, 0.61, and 0.40 emu g^{-1}, respectively. This indicated that the MCNTs could be collected successfully by applying a magnetic field after adsorption.

Adsorption kinetics of PCP on different MCNTs

To test the adsorption rate of the different MCNTs, the adsorption of PCP from aqueous solutions was carried out using the batch technique. The different MCNTs (0.05 g) were added to bottles containing 50 mL of 50 mg L^{-1} PCP solution and shaken in a constant temperature oscillator (25 °C, 180 rpm). Figure 4 shows the effect of contact time on the amount of PCP removed. The amount of PCP adsorbed by different MCNTs increased drastically in the range of 0–80 min, and finally reached equilibrium at 120 min, and the equilibrium times for the different MCNTs were not too different.

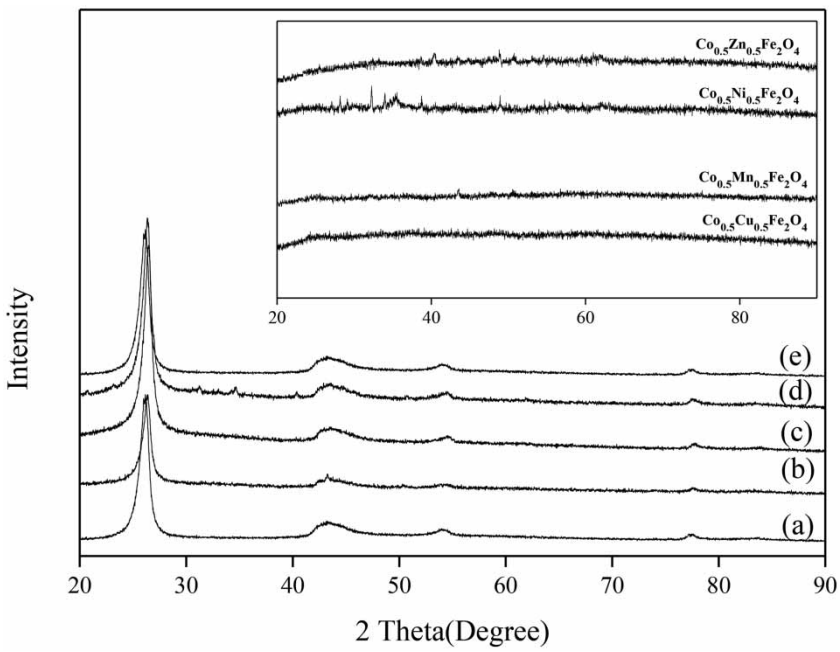

Figure 2 | XRD spectra of the different MCNTs. The main figure is MCNTs and the inset is pure magnetic nanomaterials. (a) CNTs; (b) $Co_{0.5}Cu_{0.5}Fe_2O_4$-CNTs; (c) $Co_{0.5}Mn_{0.5}Fe_2O_4$-CNTs; (d) $Co_{0.5}Ni_{0.5}Fe_2O_4$-CNTs; and (e) $Co_{0.5}Zn_{0.5}Fe_2O_4$-CNTs.

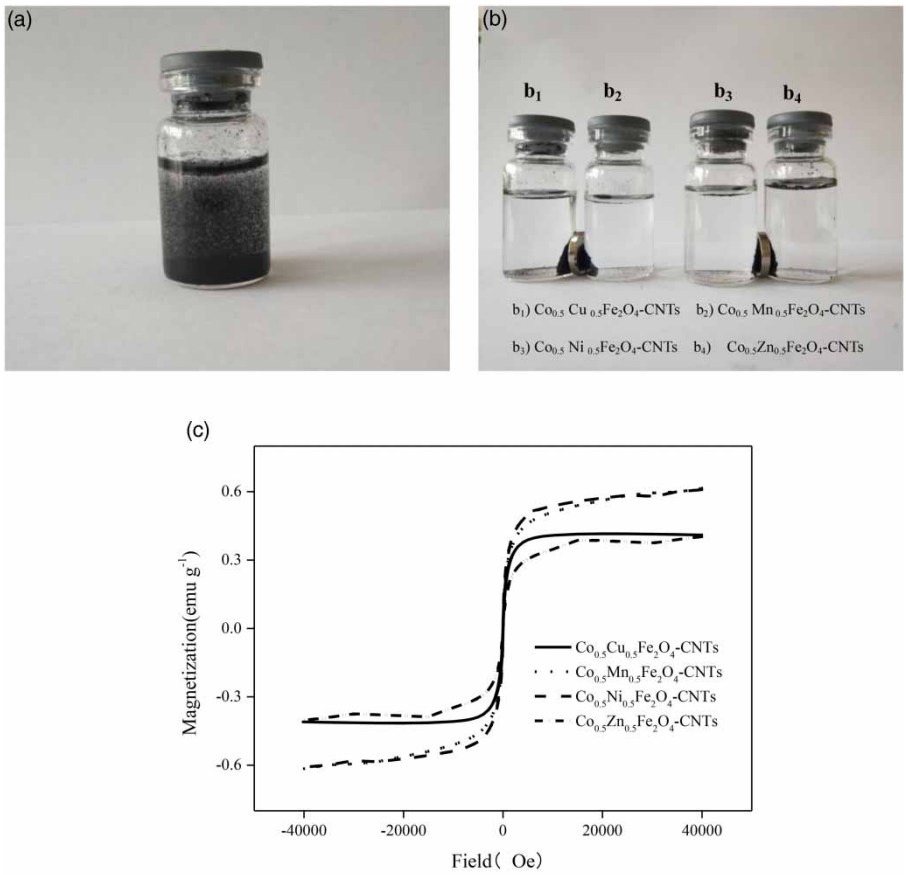

Figure 3 | Magnetic characterization of different MCNTs: (a) dispersion of MCNTs in aqueous solution; (b) magnetic response of the different MCNTs; and (c) magnetization curves at room temperature for the different MCNTs.

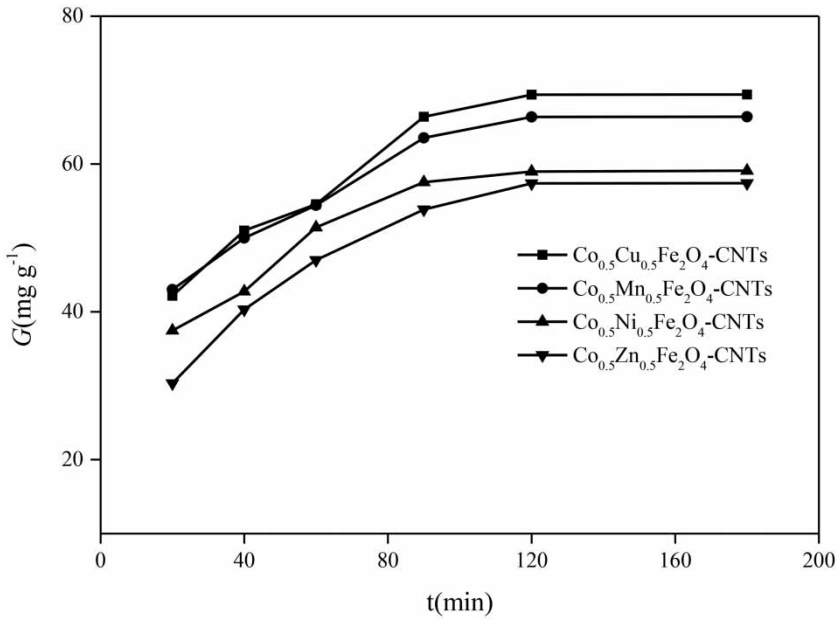

Figure 4 | Adsorption kinetic curves of PCP on different MCNTs at 25 °C.

In this study, the pseudo-first-order and pseudo-second-order kinetic models were used to evaluate the mechanism of different MCNTs for the PCP.

The pseudo-first-order adsorption kinetic model expression is (Qin *et al.* 2015):

$$\ln(G_e - G_t) = \ln G_e - k_1 t \tag{3}$$

The pseudo-second-order adsorption kinetic model expression is (Mobtaker *et al.* 2018):

$$\frac{t}{G_t} = \frac{1}{k_2 G_e^2} + \frac{1}{G_e} t \tag{4}$$

In the equations, G_t is the adsorption capacity (mg g^{-1}) at time t; G_e is the saturated adsorption amount at equilibrium (mg g^{-1}); k_1 is the quasi-first-order adsorption rate constant (min^{-1}); and k_2 is the quasi-second-order adsorption rate constant (mg (g·min)$^{-1}$). The kinetic constants obtained by fitting are shown in Table 1. According to the correlation coefficients (R^2) in Table 1, the pseudo-second-order model fitted the adsorption kinetics better than the pseudo-first-order for the investigated PCP. In addition, G_e calculated by the quasi-secondary kinetic equation was consistent with the experimental results. This indicates that physical and chemical interactions occurred between PCP and MCNTs. The adsorption capacity of the MCNTs for PCP was in the following order: $Co_{0.5}Cu_{0.5}Fe_2O_4$-CNTs > $Co_{0.5}Mn_{0.5}Fe_2O_4$-CNTs > $Co_{0.5}Ni_{0.5}Fe_2O_4$-CNTs > $Co_{0.5}Nn_{0.5}Fe_2O_4$-CNTs.

Adsorption isotherms of PCP on different MCNTs

To investigate the adsorption isotherms, the different MCNTs (0.05 g) were added to bottles containing 50 mL of PCP solution with a certain concentration and shaken in a constant temperature oscillator (25 °C, 180 rpm).

According to the equilibrium concentration and the adsorption amount, the adsorption isotherms were fitted following the Langmuir and Freundlich adsorption isotherm models.

The Langmuir adsorption isotherm model is (Hu *et al.* 2011):

$$G_e = \frac{G_m b C}{1 + bC} \tag{5}$$

The Freundlich adsorption isotherm model is (Xu *et al.* 2018):

$$G_e = k_F C^{1/n} \tag{6}$$

In Equations (5) and (6), G_e represents the equilibrium adsorption amount (mg g^{-1}); G_m represents the maximum adsorption amount (mg g^{-1}); C represents the equilibrium concentration (mg L^{-1}); b represents the adsorption equilibrium constant (L mg^{-1}); k_F is the adsorption capacity, and $1/n$ is the Freundlich constant, which indicates the rate of change with the amount of adsorption.

The obtained adsorption constants, according to the two adsorption isotherm models, are shown in Table 2.

From the correlation coefficient R^2 in Table 2, it can be seen that the Langmuir equation and the Freundlich equation described the adsorption of PCP on MCNTs. The results showed that the monolayer and multilayer adsorption were simultaneously occurring adsorption. From the fitting, the maximum adsorption amount (G_m) of $Co_{0.5}Cu_{0.5}Fe_2O_4$-CNTs, $Co_{0.5}Mn_{0.5}Fe_2O_4$-CNTs, $Co_{0.5}$ $Ni_{0.5}Fe_2O_4$-CNTs, and $Co_{0.5}Zn_{0.5}Fe_2O_4$-CNTs was 76.02, 75.80, 75.83, and 74.50 mg g^{-1}, respectively. In addition, $1/n$ is related to the strength of the adsorption driving force. When $0.1 < 1/n < 0.5$, adsorption was easy; when $0.5 < 1/n \leq 1$, the adsorption process was a little difficult; and when $1/n > 1$, the adsorption process was very difficult (Yu *et al.* 2018). The values of $1/n$ for PCP on the different MCNTs were less than 0.5, which demonstrated that PCP could be quite easily adsorbed on the MCNTs.

Table 1 | Adsorption kinetic constants of different MCNTs

		Pseudo-first-order kinetic model			Pseudo-second-order kinetic model		
MCNTs type	$G_{e,exp}$ (mg g^{-1})	$G_{e,cal}$ (mg g^{-1})	k_1 (min^{-1})	R^2	$G_{e,cal}$ (mg g^{-1})	k_2 (mg g^{-1} min^{-1})	R^2
$Co_{0.5}Cu_{0.5}Fe_2O_4$-CNTs	70.48	32.78	3.75	0.85	70.59	0.016	0.90
$Co_{0.5}Mn_{0.5}Fe_2O_4$-CNTs	67.48	45.08	3.57	0.87	67.59	0.016	0.93
$Co_{0.5}Ni_{0.5}Fe_2O_4$-CNTs	60.20	45.95	3.37	0.84	60.30	0.018	0.93
$Co_{0.5}Nn_{0.5}Fe_2O_4$-CNTs	58.48	40.05	3.65	0.87	58.49	0.019	0.86

Table 2 | Adsorption isotherm fitting constants of different MCNTs for PCP

		Langmuir			Freundlich		
MCNTs type	**Surface area ($m^2 g^{-1}$)**	G_m	b	R^2	k_F	$1/n$	R^2
$Co_{0.5}Cu_{0.5}Fe_2O_4$-CNTs	112.04	76.02	0.10	0.96	20.38	0.30	0.98
$Co_{0.5}Mn_{0.5}Fe_2O_4$-CNTs	108.20	75.80	0.09	0.99	18.46	0.31	0.98
$Co_{0.5}Ni_{0.5}Fe_2O_4$-CNTs	95.52	75.83	0.06	0.98	14.33	0.36	0.97
$Co_{0.5}Zn_{0.5}Fe_2O_4$-CNTs	96.05	74.50	0.05	0.99	11.93	0.38	0.99

Effect of pH on PCP adsorption

The solution pH can affect the surface charge of the MCNT and ionized forms of PCP, which will further affect the adsorption. According to zeta potential detection, the pH value of zero charge of different MCNTs was about 5. At $pH \leq 5$, the MCNTs surface charge was positive, and at $pH > 5$, the surface charge was negative. In addition, the pH affects the ionized forms of PCP in water. PCP is a weak acid, as shown in Equation (7), and the dissolution of PCP in water will result in two chemical forms, undissociated (C_6CI_5OH) and the pentachlorophenoxide anion ($C_6Cl_5O^-$). The ratio of these components changes with pH. When the pH is increased, the amount of C_6CI_5OH will decrease. According to literature reports (Arcand *et al.* 1995), at $pH \leq 3$ approximately 95% of the content will be un-ionized (C_6CI_5OH) and at $pH > 4$, the $C_6Cl_5O^-$ content will increase significantly as the pH is increased, with approximately 98% of PCP dissociating into the pentachlorophenoxide anion ($C_6Cl_5O^-$) at pH 6.

$$C_6Cl_5OH + H_2O \rightarrow C_6Cl_5O^- + H_3O^+ \quad (7)$$

To investigate the pH effect on adsorption, the different MCNTs were added to a PCP solution with pH values of 2–10 and shaken for 2 h to reach adsorption equilibrium. Figure 5 shows that the adsorption capacity of PCP was remarkably dependent on the solution pH and this trend was the same for the different MCNTs. When the solution pH was increased from 2 to 5, the adsorption capacity of PCP remained stable, but at a pH 5–12, the adsorption capacity was markedly reduced. We attributed this result to when $pH \leq 4.9$, the MCNT's surface exhibited a positive charge and the PCP mostly existed in an un-ionized molecular state (C_6CI_5OH). The pH change, therefore, did not affect the adsorption capacity. When $pH > 5$, the MCNT's surface exhibited a negative charge and the ionized state content of $C_6Cl_5O^-$ increased significantly with an increase of pH. When $pH > 5$, electrostatic repulsion existed between the MCNT's surface and the $C_6Cl_5O^-$, and so the adsorption capacity was significantly reduced.

Effect of temperature on PCP adsorption

To study the effect of temperature on adsorption, the adsorption experiments were performed at different temperatures. The different MCNTs (0.03 g) were added to bottles containing 50 mL of PCP and shaken at temperatures of 20 °C, 30 °C, 40 °C, and 50 °C. Figure 6 shows the adsorption capacities of the $Co_{0.5}Cu_{0.5}Fe_2O_4$-CNTs, $Co_{0.5}Mn_{0.5}Fe_2O_4$-CNTs, $Co_{0.5}Ni_{0.5}Fe_2O_4$-CNTs, and $Co_{0.5}Zn_{0.5}Fe_2O_4$-CNTs were 43.2, 40.8, 35.1, and 33.9 mg g^{-1} at 20 °C, respectively. When the temperature was increased from 20 °C to 50 °C, the adsorption capacities of the MCNTs for PCP were noticeably reduced. The adsorption capacities of the $Co_{0.5}Cu_{0.5}Fe_2O_4$-CNTs, $Co_{0.5}Mn_{0.5}Fe_2O_4$-CNTs, $Co_{0.5}Ni_{0.5}$-Fe_2O_4-CNTs, and $Co_{0.5}Zn_{0.5}Fe_2O_4$-CNTs were reduced to 26.5, 25.9, 22.8, and 20.7 mg g^{-1} at 50 °C, respectively.

In addition, the thermodynamic parameters of the adsorption process were calculated according to the thermodynamic formulas and Van 't Hoff Equations (8) and (9).

$$\Delta G = -RT\ln K_e \quad (8)$$

$$\ln K_e = \frac{\Delta S}{R} - \frac{\Delta H}{RT} \quad (9)$$

where ΔG is the standard free energy change (kJ mol^{-1}); R the universal gas constant (8.314 J mol^{-1} K); T is the absolute temperature (K); K_e is the Langmuir equilibrium constant (L g^{-1}), $K_e = G_e/C_e$; ΔH is the enthalpy change (kJ mol^{-1}), ΔS is the entropy change (J ($mol \cdot K^{-1}$)).

The thermodynamic relative parameters are summarized in Table 3. The negative values of enthalpy changes (ΔH) indicated that the adsorption process was exothermic. The negative values of entropy changes (ΔS) indicated that the randomness at the interface between the adsorbent

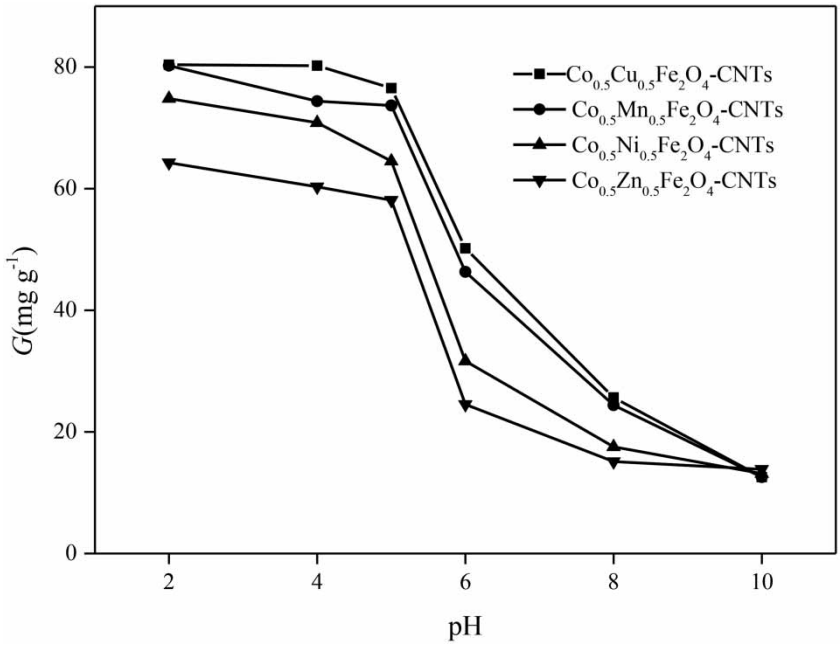

Figure 5 | Effect of pH on the adsorption capacity of PCP on MCNTs.

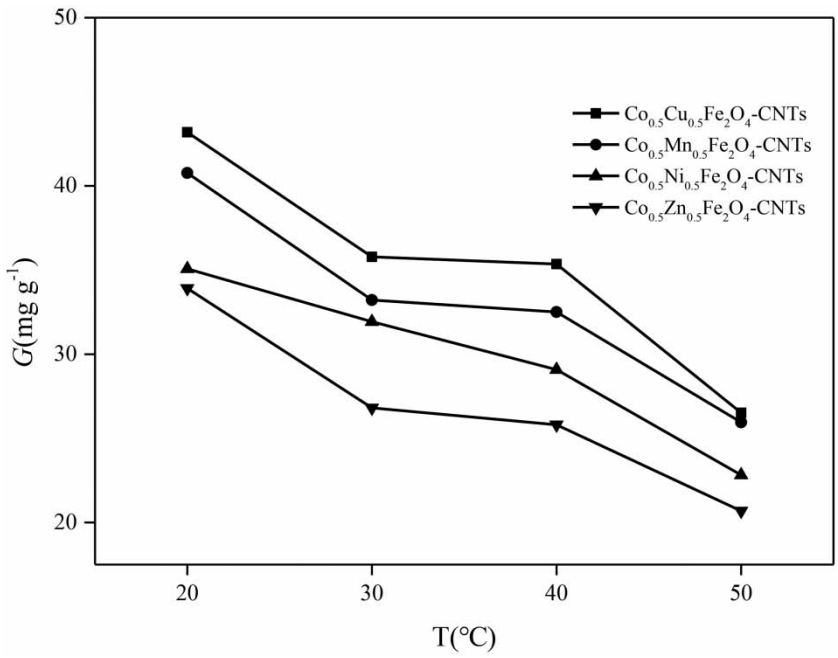

Figure 6 | Effect of temperature on the adsorption capacity of PCP on different MCNTs.

and the solution was reduced due to adsorption, and there was no significant change in the internal structure of the adsorbent after adsorption (Liu *et al.* 2015). All results clearly indicate that the reaction was mainly based on physical adsorption, and a high adsorption capacity can be achieved at room temperature with no additional conditions required, which saves energy for practical applications and allowing this process to be widely applied.

Table 3 | Thermodynamic parameters of PCP adsorption by MNCNTs

	ΔG (kJ mol^{-1})					
MCNTs type	**293 K**	**303 K**	**313 K**	**323 K**	**ΔH (kJ mol^{-1})**	**ΔS (kJ mol^{-1})**
$Co_{0.5}Cu_{0.5}Fe_2O_4$-CNTs	−1.073	−0.4307	0.2113	0.8532	−19.884	−64.19
$Co_{0.5}Mn_{0.5}Fe_2O_4$-CNTs	−1.226	−0.6172	−0.1788	0.6014	−19.08	−60.93
$Co_{0.5}Ni_{0.5}Fe_2O_4$-CNTs	−0.5708	−0.02604	0.05188	1.064	−16.53	−54.48
$Co_{0.5}Zn_{0.5}Fe_2O_4$-CNTs	−0.5996	0.03358	0.06668	1.300	−19.15	−63.32

Microwave regeneration

Figure 7 shows complex permittivity and complex magnetic permeability of the different MCNTs in the 2–18 GHz band.

The real part of the complex permittivity (e') and the real part of the complex permeability (μ') represent the ability to store electric energy and magnetic energy, and the imaginary part of the complex permittivity (e'') and the imaginary part of the complex permeability (μ'') represent the ability to lose electric energy and magnetic energy (Zhang *et al.* 2013). Figure 7 shows that the e' and e'' of the four MCNTs in the range of 2–10 GHz gradually decreased with increasing frequency. At 10–18 GHz, the real and imaginary parts of $Co_{0.5}Ni_{0.5}Fe_2O_4$-CNTs and $Co_{0.5}Zn_{0.5}Fe_2O_4$-CNTs exhibited a stable trend. $Co_{0.5}Cu_{0.5}Fe_2O_4$-CNTs showed a resonance peak in the range of 10–12 GHz, and $Co_{0.5}Mn_{0.5}Fe_2O_4$-CNTs showed a resonance peak in the range of 12–15 GHz. This phenomenon was attributed to the hysteresis response of the dipole polarization under the high frequency variation of the electric field. In addition, the μ' and μ'' of the four kinds of MCNTs fluctuated greatly, and the μ' and μ'' of $Co_{0.5}Mn_{0.5}Fe_2O_4$-CNTs and $Co_{0.5}Zn_{0.5}Fe_2O_4$-CNTs reached a maximum near 12 GHz and reached a minimum near 14 GHz. The μ' of $Co_{0.5}Cu_{0.5}Fe_2O_4$-CNTs showed a resonance peak near 12–15 GHz, and the μ'' value showed a resonance peak near 14–16 GHz. The above phenomena were due to the combination of the dispersion effect and the polarization effect.

If the e'' value is greater than the μ'' value, it indicates that the adsorbent is an electric loss-absorbing medium; if the μ'' value is greater than the e'' value, it indicates that the adsorbent is a magnetic loss-absorbing medium (Hou *et al.* 2013). Figure 7 shows that the e'' value was much larger than the μ'' value, which indicated that these four magnetic carbon nanotubes are electric loss-type microwave absorbing media (Zeng *et al.* 2012). In summary, the four MCNTs exhibit good wave absorbing properties at low frequencies. Therefore, adsorption saturation of PCP on different MCNTs is suitable for microwave regeneration. At 850 W, the temperature of MCNTs quickly reaches 1,100 °C within 100 s.

In this study, we selected microwave irradiation at 850 W for 180 s for the degradation of the adsorption-saturated PCP on different MCNTs. According to the analysis of the combined substances of the MCNT extraction and distillation, the degradation and mineralization efficiencies were over 90%. The relationship between the regeneration times and the regeneration efficiency is shown in Figure 8. The regeneration efficiency of MCNTs was basically stable with the

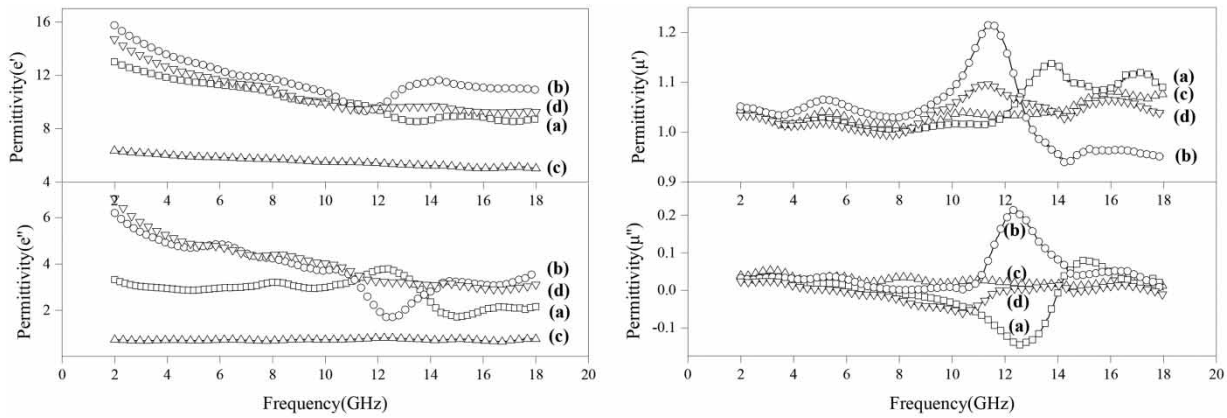

Figure 7 | Complex permittivity and complex magnetic permeability of different MCNTs in the 2–18 GHz band: (a) $Co_{0.5}Cu_{0.5}Fe_2O_4$-CNTs; (b) $Co_{0.5}Mn_{0.5}Fe_2O_4$-CNTs; (c) $Co_{0.5}Ni_{0.5}Fe_2O_4$-CNTs; and (d) $Co_{0.5}Zn_{0.5}Fe_2O_4$-CNTs.

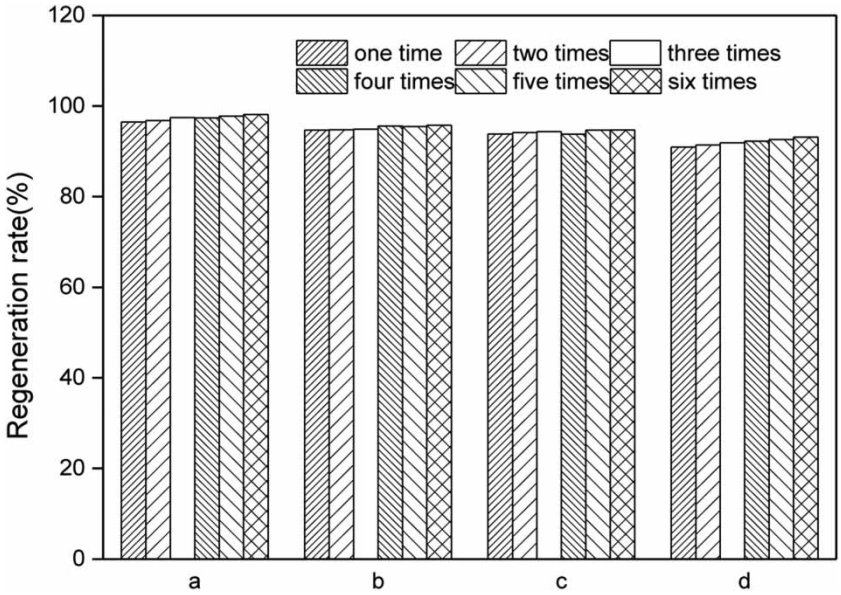

Figure 8 | Relationship between the regenerative efficiency with reuse cycles of PCP on different MCNTs: (a) $Co_{0.5}Cu_{0.5}Fe_2O_4$-CNTs; (b) $Co_{0.5}Mn_{0.5}Fe_2O_4$-CNTs; (c) $Co_{0.5}Ni_{0.5}Fe_2O_4$-CNTs; and (d) $Co_{0.5}Zn_{0.5}Fe_2O_4$-CNTs.

increase of regeneration times, and had high regeneration efficiency. Under the same conditions, the regeneration efficiency of $Co_{0.5}Cu_{0.5}$ Fe_2O_4-CNTs, $Co_{0.5}Mn_{0.5}Fe_2O_4$-CNTs, $Co_{0.5}Ni_{0.5}$ Fe_2O_4-CNTs, and $Co_{0.5}Zn_{0.5}Fe_2O_4$-CNTs were still 98.1%, 95.8%, 93.1%, and 94.7%, respectively, after six cycles of microwave regeneration. In addition, after reuse six times, the loss of magnetic materials was less than 7%.

CONCLUSIONS

In this study, $Co_{0.5}M_{0.5}Fe_2O_4$ (M = Ni, Cu, Mn, Zn)-CNTs were successfully prepared using the solvothermal method with high specific surface area, good magnetic properties, and absorption microwave characteristics. The adsorption kinetics and isotherms of PCP on $Co_{0.5}M_{0.5}Fe_2O_4$-CNTs demonstrated that $Co_{0.5}M_{0.5}Fe_2O_4$ has the advantages of fast adsorption equilibrium and large adsorption capacity, and the adsorption capacity is sensitive to pH and temperature. The influencing factors of the acidity condition and low temperature are most favorable for adsorption. In addition, $Co_{0.5}M_{0.5}Fe_2O_4$-CNTs exhibits good microwave absorption properties at low frequencies. After magnetic recovery of the saturated $Co_{0.5}M_{0.5}Fe_2O_4$-CNTs, they can be rapidly regenerated by microwave regeneration with no secondary pollution. After six adsorption and microwave treatment cycles, the regeneration efficiency remains at 98% and no apparent damage is observed to the structure. Therefore, these $Co_{0.5}M_{0.5}Fe_2O_4$-CNTs are suitable for the combination of adsorption, magnetic recovery, and microwave degradation to treat organic pollutants in water.

ACKNOWLEDGEMENTS

This work was supported financially by the Nature Science Foundation (No. 51678323) and Shandong Provincial Science Foundation (No. ZR2017MEE013) of China. We thank Liwen Bianji, Edanz Group China (www.liwenbianji.cn/ac), for editing the English text of a draft of this manuscript.

REFERENCES

Alfaya, E., Iglesias, O., Pazos, M. & Sanroman, M. A. 2015 Environmental application of an industrial waste as catalyst for the electro-Fenton-like treatment of organic pollutants. *RSC Advances* **5** (19), 14416–14424.

Arcand, Y., Hawari, J. & Guiot, S. 1995 Solubility of pentachlorophenol in aqueous solutions: the pH effect. *Water Research* **29** (1), 131–136.

Bhanjana, G., Dilbaghi, N., Kim, K.-H. & Kumar, S. 2017 Carbon nanotubes as sorbent material for removal of cadmium. *Journal of Molecular Liquids* **242**, 966–970.

Cui, C. Y., Xie, Q., Yu, H. T., Han, Y. H. & Chen, S. 2008 Electrocatalytic hydrodechlorination of pentachlorophenol at palladium multiwalled carbon nanotubes electrode. *Applied Catalysis B: Environmental* **80** (1–2), 122–128.

Cui, C. Y., Zheng, Q. Z., Han, Y. H. & Xin, Y. J. 2015 Rapid microwave-assisted regeneration of magnetic carbon nanotubes loaded with p-nitrophenol. *Applied Surface Science* **346**, 9–106.

Gao, H. J., Zhao, S. Y. & Cheng, X. Y. 2013 Removal of anionic azo dyes from aqueous solution using magnetic polymer multi-wall carbon nanotube nanocomposite as adsorbent. *Chemical Engineering Journal* **223**, 84–90.

Hou, C. L., Li, T. H. & Zhao, T. K. 2013 Electromagnetic wave absorbing properties of multi-wall carbon nanotube/Fe_3O_4 hybrid materials. *New Carbon Materials* **28** (3), 184–190.

Hu, X. B., Liu, B. Z. & Deng, Y. H. 2011 Adsorption and heterogeneous Fenton degradation of 17α-methyltestosterone on nano Fe_3O_4/MWCNTs in aqueous solution. *Applied Catalysis B: Environmental* **107** (3–4), 274–283.

Kahar, S. M., Voon, C. H., Lee, C. C. & Gopinath, S. C. B. 2017 Synthesis of silicon carbide nanowhiskers by microwave heating: effect of heating duration. *Materials Research Express* **4** (1), 015005.

Kaiser, M. 2012 Electrical conductivity and complex electric modulus of titanium doped nickel-zinc ferrites. *Physica B: Condensed Matter* **407** (4), 606–613.

Li, G., Sheng, L. M., Yu, L. M., An, K., Ren, W. & Zhao, X. L. 2015 Electromagnetic and microwave absorption properties of single-walled carbon nanotubes and $CoFe_2O_4$ nanocomposites. *Materials Science and Engineering B* **193**, 153–159.

Liu, X., Leng Y, B., Gu S, Y. & Zhang, Z. Z. 2015 Adsorption of hexavalent chromium in aqueous solution by rapeseed straw shell. *China Environmental Science* **35** (6), 1740–1748.

Mobtaker, H. G., Pakzad, S. M. & Yousefi, T. 2018 Magnetic CuHCNPAN nano composite as an efficient adsorbent for strontium uptake. *Journal of Nuclear Materials* **504**, 55–60.

Mohammadi, A. & Veisi, P. 2018 High adsorption performance of β-cyclodextrin-functionalized multi-walled carbon nanotubes for the removal of organic dyes from water and industrial wastewater. *Journal of Environmental Chemical Engineering* **6** (4), 4634–4643.

Peng, X. J., Luan, Z. K. & Di, Z. C. 2005 Carbon nanotubes-iron oxides magnetic composites as adsorbent for removal of Pb(II) and Cu(II) from water. *Carbon* **43** (4), 855–894.

Peng, P., Lang, Y. H. & Wang, X. M. 2016 Adsorption behavior and mechanism of pentachlorophenol on reed biochars: pH effect, pyrolysis temperature, hydrochloric acid treatment and isotherms. *Ecological Engineering* **90** (5), 225–233.

Qi, C., Liu, X., Lin, C., Zhang, H., Li, X. & Ma, J. 2017 Activation of peroxymonosulfate by microwave irradiation for degradation of organic contaminants. *Chemical Engineering Journal* **315**, 201–209.

Qin, J., Qiu, F., Rong, X., Yan, J., Zhao, H. & Yang, D. 2015 Adsorption behavior of crystal violet from aqueous solutions with chitosan-graphite oxide modified polyurethane as an adsorbent. *Journal Applied Polymer Science* **132** (7), 418–428.

Shao, D. D., Sheng, G. D. & Chen, C. G. 2010 Removal of polychlorinated biphenyls from aqueous solutions using β-cyclodextrin grafted multiwalled carbon nanotubes. *Chemosphere* **79** (7), 679–685.

Wang, P. F., Cao, M. H., Wang, C., Ao, Y. H., Hou, J. & Qian, J. 2014 Kinetics and thermodynamics of adsorption of methylene blue by a magnetic graphene-carbon nanotube composite. *Applied Surface Science* **290**, 116–124.

Weavers, L. K., Almstadt, N. & Hoffmann, M. R. 2000 Kinetics and mechanism of pentachlorophenol degradation by sonication, ozonation, and sonolytic ozonation. *Environmental Science Technology* **34** (7), 1280–1285.

Wen, F. S., Zhang, F. & Xiang, J. Y. 2013 Microwave absorption properties of multiwalled carbon nanotube/FeNi nanopowders as light-weight microwave absorbers. *Journal of Magnetism and Magnetic Materials* **343**, 281–285.

Xiao, D. L., Li, H., He, H., Lin, R. & Zuo, P. L. 2014 Adsorption performance of carboxylated multi-wall carbon nanotube-Fe_3O_4 magnetic hybrids for Cu(II) in water. *Carbon* **71**, 343–349.

Xu, J., Cao, Z. & Zhang, Y. L. 2018 A review of functionalized carbon nanotubes and graphene for heavy metal adsorption from water: preparation application, and mechanism. *Chemosphere* **195**, 351–364.

Yan, W. N., Bian, W. Y., Jin, C., Tian, J. H. & Yang, R. Z. 2015 An efficient Bi-functional electrocatalyst based on strongly coupled $CoFe_2O_4$/carbon nanotubes hybrid for oxygen reduction and oxygen evolution. *Electrochimica Acta* **177**, 65–72.

Ye, M., Chen, Z., Wang, W., Shen, J. & Ma, J. 2010 Hydrothermal synthesis of TiO_2 hollow microspheres for the photocatalytic degradation of 4-chloronitrobenzene. *Journal of Hazardous Materials* **184**, 612–619.

Yu, Y., Yu, L., Shih, K. & Chen, J. P. 2018 Yttrium-doped iron oxide magnetic adsorbent for enhancement in arsenic removal and ease in separation after applications. *Journal of Colloid and Interface Science* **521**, 252–260.

Zeng, J., Fan, H. Q. & Wang, Y. L. 2012 Ferromagnetic and microwave absorption properties of copper oxide/cobalt/carbon fiber multilayer film composites. *The Solid Films* **520**, 5053–5059.

Zhan, Y. Q., Zhao, R., Lei, Y. J., Meng, F. B., Zhong, J. C. & Liu, X. B. 2011 A novel carbon nanotubes/Fe_3O_4 inorganic hybrid material: synthesis, characterization and microwave electromagnetic properties. *Journal of Magnetism and Magnetic Materials* **323** (7), 1006–1010.

Zhang, T., Huang, D. Q. & Yang, Y. 2013 Fe_3O_4/carbon composite nanofiber absorber with enhancedmicrowave absorption performance. *Materials Science and Engineering B* **178**, 1–9.

Zhu, L., Lin, H. Z., Jiao-Qin, Q., Xu, X. Y. & Qi, H. Y. 2012 Effect of H_2 on reductive transformation of p-ClNB in a combined ZVI–anaerobic sludge system. *Water Research* **46** (19), 6291–6299.

First received 28 October 2019; accepted in revised form 22 March 2020. Available online 2 April 2020